Journal of the Earth & Space Physics. Vol. 38, No. 2, 2012, P. 17-28

Seismic study of upper mantle beneath the NW Iran using P receiver function

Taghizadeh-Farahmand, F.[1*], Sodoudi, F.[2] and Afsari, N.[3]

[1] *Assistant Professor, Department of Physics, Qom Branch, Islamic Azda University, Qom, Iran*
[2] *Helmholtz Center Potsdam, GFZ Research Center for Geosciences, Potsdam, Germany*
[3] *Assistant Professor, Department of Civil Engineering, Noshahr Branch, Islamic Azad University, Noshahr, Iran*

(Received: 19 May 2010, Accepted: 31 Jan 2012)

Abstract

RF method is now a well-known tool for studying crustal and upper mantle structure when such a complete data set is available. We compute P receiver functions to investigate the upper mantle discontinuity beneath the Northwest of Iran. We selected data from teleseismic events (Mb ≥ 5.5, 30 °>△ > 95°) recorded from 1995 to 2008 at 8 three component short period stations from Tabriz Telemetry Seismic Network with high signal-to-noise ratio. The P to S converted phases from 410 and 660 km discontinuities are delayed by more 2 and 1 s with respect to IASP91 global reference model, indicating that the upper mantle above 410 km is 3-4% slower and high temperature than the standard earth model. Because the 410 and 660 km discontinuities do not show the same delay, the transition zone is also could be thinner. This could mean that the upper mantle in the region is still influenced by several geodynamical processes involving rifting, uplift and magmatism.

Key words: P receiver functions, Teleseismic, Upper mantle, Transitoin zone

بررسی لرزه‌ای گوشته بالایی در زیر شمال‌غرب ایران با استفاده از تابع گیرنده P

فتانه تقی‌زاده فرهمند [۱*]، فروغ صدودی [۲] و نرگس افسری [۳]

[۱] *استادیار، دانشگاه آزاد اسلامی واحد قم، گروه فیزیک، قم، ایران*
[۲] *پژوهشگر، مؤسسه تحقیقاتی علوم زمین هلمهولتز، پستدام، آلمان*
[۳] *استادیار، دانشگاه آزاد اسلامی واحد نوشهر، گروه عمران، نوشهر، ایران*

(دریافت: ۸۹/۲/۲۹ ، پذیرش نهایی: ۹۰/۱۱/۱۱)

چکیده

تابع گیرنده P روش مفیدی برای بررسی ساختار پوسته و گوشته بالایی زمین است. در این تحقیق به کمک تحلیل تابع گیرنده P و با استفاده از زمان رسید فاز تبدیلی Ps در ناپیوستگی‌های گوشته بالایی(۴۱۰ و ۶۶۰ کیلومتری)، منطقه انتقالی گوشته مورد بررسی قرار گرفت. برای این منظور داده‌های بیش از ۳۵۰ زمین‌لرزه دورلرز ثبت شده در ۸ ایستگاه ثابت کوتاه‌دوره شبکه لرزه‌نگاری تبریز واقع در شمال‌غرب ایران از ۱۹۹۵ تا ۲۰۰۸ با بزرگای $M_b \geq$ ۵/۵ و در فاصله رومرکزی °۹۵> Δ <°۳۰مورد پردازش قرار گرفت. به‌منظور محاسبه تابع گیرنده پس از حذف اثر دستگاهی، مؤلفه‌های ZNE تحت زاویه Back Azimuth و زاویه تابش موج فرودی چرخانده شدند تا به دستگاه مختصات محلی پرتوLQT تبدیل شوند. برای حذف اثرات چشمه و مسیر انتشار مؤلفه Q با سیگنال P روی مؤلفه L واهمامیخت (Deconvolve) می‌شود، نتیجه به‌دست آمده روی مؤلفه Q، تابع گیرنده P نامیده می‌شود. با استفاده از اختلاف زمان رسید فازهای تبدیلی Ps از ناپیوستگی‌های گوشته بالایی نسبت به رسید مستقیم P در روش تابع گیرنده P می‌توان عمق ناپیوستگی‌ها را در گوشته محاسبه کرد. به دلیل پراکندگی، تضعیف و عبور از گوشته بالایی ناهمگن و پوسته، فازهای تبدیلی از

*Corresponding author: Tel: 0912-2384270 Fax: 0251-28005797 E-mail: f_farahmand@qom-iau.ac.ir

ناپیوستگی‌های گوشته ضعیف تر از فازهای تبدیلی از ناپیوستگی موهو است و برانبارش تابع‌ها گیرنده به مشاهده واضح‌تر آنها کمک می‌کند. ابتدا پنجره زمانی به طول ۱۱۰ ثانیه (۱۰ ثانیه قبل از شروع موج P) از نگاشت‌های خام سرعت با نسبت سیگنال به نوفه بالا انتخاب شد. با توجه به کوتاه‌دوره بودن داده‌ها و دارا بودن پاسخ بسامدی ۱ هرتز از فیلتر میان‌گذر ۰/۳ ثانیه تا ۱۰ ثانیه استفاده شد. واهمامیخت روی داده‌ها با مقادیر متفاوت برای Water Level (۰/۰۰۱ تا ۱) صورت گرفت که با توجه به داده‌های موجود، مناسب‌ترین مقدار ۰/۰۱ انتخاب شد. فیلتر پایین‌گذر ۵ ثانیه روی تابع‌های گیرنده P محاسبه شده در همهٔ ایستگاه‌های شبکه تبریز به‌کار گرفته شد. با تهیه مقطع دوبُعدی عمق-مسافت، در مقطع شرقی- غربی در امتداد °۳۸ عرض شمالی، مدل متوسطی از ساختار زمین در منطقه انتقالی به‌دست آمد. برای وضوح بهتر تبدیلات تابع گیرندهP محاسبه شده، آنها را برحسب عرض جغرافیایی نقاط تبدیل مرتب ساخته و سپس منطقه مورد بررسی را در شبکه‌های به طول ۰/۰۹ درجه با هم‌پوشانی ۰/۰۵ درجه دسته‌بندی کرده‌ایم. قبل از برانبارش کل تابع‌ها تصحیح دینامیکی صورت گرفت. با توجه به برانبارش تابع‌های گیرنده در منطقه انتقالی گوشته زمان رسید فازهای تبدیلی از ناپیوستگی‌های ۴۱۰ و ۶۶۰ کیلومتری تأخیر در رسید را نشان دادند. فازهای تبدیلی از هر دو ناپیوستگی نسبت به مدل متوسط جهانی IASP91 با تأخیر زمانی به‌ترتیب ۲ و ۱ ثانیه دریافت شد. اختلاف زمان‌های رسید به‌دست آمده از دامنه فازهای تبدیلی از دو ناپیوستگی منطقه انتقالی گوشته برابر ۲۳ ثانیه است که این اختلاف نسبت به متوسط جهانی(۲۴ ثانیه)، ۱ ثانیه کمتر است. نبود تأخیر یکسان در رسید می‌تواند بیانگر ضخامت کمتر منطقه انتقالی در زیر منطقه شمال‌غرب باشد، که احتمالاً ناشی از بی‌هنجاری دمایی (دمای بالاتر نسبت به محیط اطراف) اس و موجب کاهش سرعت‌های لرزه‌ای (Vp,Vs) می‌شود. با توجه به اینکه در این تحقیق تغییرات دمایی زیادی بین دو ناپیوستگی (۴۱۰ و ۶۶۰ کیلومتری) منطقه انتقالی وجود ندارد، می‌توان علت تأخیر در زمان رسید فازهای تبدیلی از دو ناپیوستگی (۴۱۰ و ۶۶۰ کیلومتری) را سرعت کم امواج در گوشته بیان کرد.

واژه‌های کلیدی: شمال‌غرب ایران، تابع گیرنده، گوشته بالایی و منطقه انتقالی

1 INTRODUCTION

Iran is located as a part of the Alpine-Himalaya an orogenic belt. The region referred in this study as northwest Iran is enclosed between 45˚-48˚ east longitudes and 37˚-39˚ north latitudes (Fig. 1). This region is one of seismologically active regions in the Middle-East and has experience many destructive earthquakes (Ghietanchi et al., 2004). This area was appeared with closure of Neotethys Ocean and with collision of Arabian plate and central Iran block and deformation. Northwest Iran is situated between two thrust belts; the Caucasus to the North and the Zagros Mountain belt to the South (Hessami et al., 2003). Deformation and seismicity in this region is mainly due to the continental shortening of the Iranian plate between the Eurasian and Arabian plates. Two prominent Neogene-Quaternary volcano mountains (Sahand and Sabalan) are located in this region (Figure 1).

The mantle transition zone marks the transition from the upper to the lower mantle. Its characteristics are important for our understanding of Earth's dynamics. Over the past decades, a number of seismic studies have demonstrated the global existence of these discontinuities and have mapped their topography (e.g. Shearer and Masters, 1992; Flanagan and Shearer, 1998a; Gossler and Kind, 1996; Gu, et al., 1998). However, the 410 is usually more difficult to detect than the 660 due to its smaller velocity contrast and to a regional strong topography, which makes observations in long period data rather difficult (Bina and Helffrich, 1994; Rost and Weber, 2002; Flanagan and Shearer, 1998b). Furthermore, a weaker discontinuity at 520 km depth has been observed locally (Shearer, 1990, 1996; Gaherty et al., 1999; Gossler and Kind, 1996; Deuss and Woodhouse, 2001). According to the IASP91 velocitymodel (Kennet and Engdahl, 1991), the velocity increase at the 410 is +3.6% for P waves and +4.1% for S waves. At the 660 it is +5.8% for P waves and +6.3% for S waves. The two main seismic discontinuities in the mantle at 410 and 660 km depth are most probably pressure-induced phase transformations in peridotite rather than a change in chemical composition. Experiments in the mid-1960s (Ringwood and Major, 1966) showed that:

1) The 410 km discontinuity is associated with the transition from Olivine to Wadsleyite (spinel-β phase). The reaction is:

(Mg,Fe)2SiO4 → (Mg,Fe)2SiO4
Olivine (α) Wadsleyite (β)

2) The 660 km discontinuity is generally believed to represent the transition from ringwoodite (spinel γ-phase) to a Perovskite and Magnesiowustite structure. The reaction is:

(Mg,Fe)2SiO4 → (Mg,Fe)O + (Mg,Fe)SiO3
Olivine (γ) Magnesiowustite+ Perovskite

Highpressure mineral-physics studies have shown that transition zone minerals at average mantle temperatures have anomalously high water solubility relative to upper-mantle minerals. Water solubility of the mantle transition zone is about 10-30 times higher than that in the upper and probably lower mantles (Bercovici and Karato, 2003). Their equilibrium depths depend on the ambient mantle temperature and pressure conditions, described by the Clayperon slpoe (Li et al., 2003). If ΔH and ΔV are the heat and volume changes resulting from the phase change, then a change dT in tempreture moves the phase change by a pressure dP given by the Clayperon slop:

$$\lambda = \frac{dP}{dT} = \frac{\Delta H}{T \Delta V} \tag{1}$$

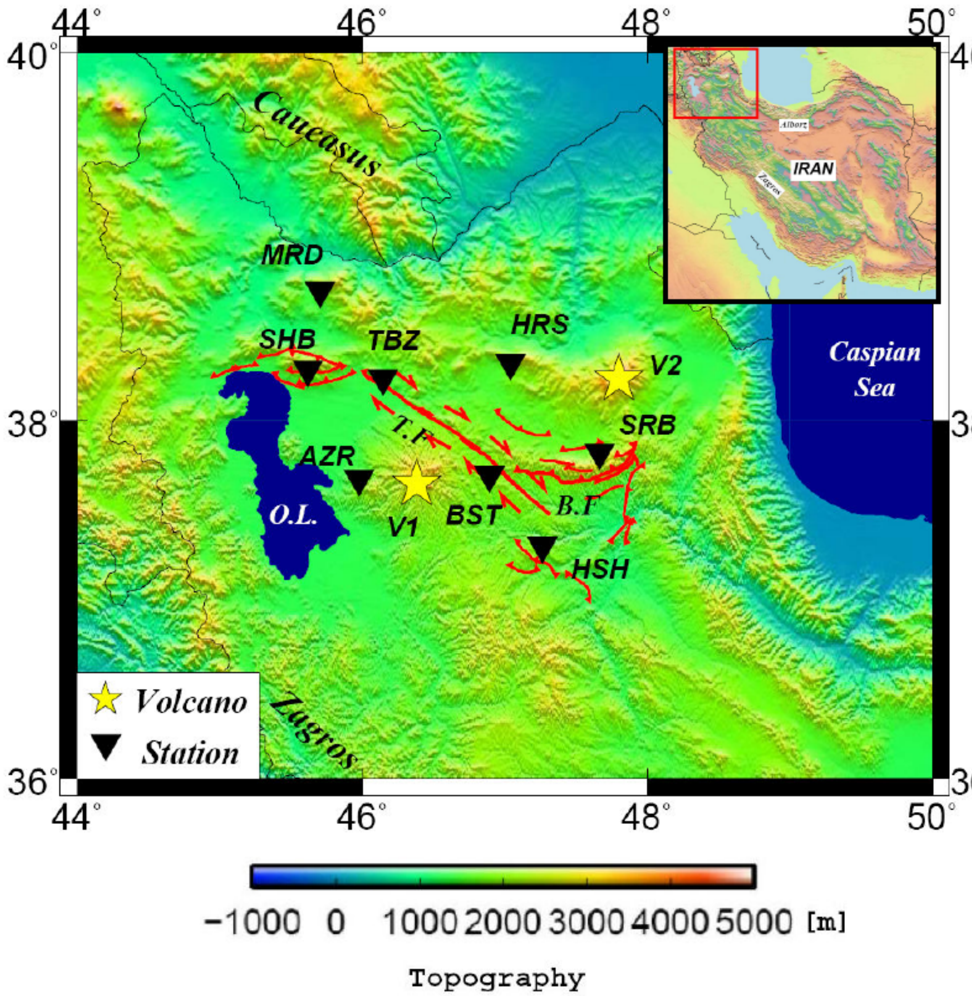

Figure1. Location map of the seismological stations (triangle) used in this study. The main faults are shown by the red lines. The yellow stars show volcano.V1: Sahand Volcano, V2: Sabalan Volcano, O.L.: Orumiyeh Lake, TBZ.F: Tabriz Fault, BG.F: Bozghosh Fault.

The transformations at the 410 and 520 have positive Clapeyron slopes, with dP/dT of approximately +3 MPa K^{-1} and +4 MPa K^{-1}, respectively. In contrast, the breakdown of ringwoodite to perovskite plus magnesiowüstite at the 660 has a negative slope of -2 MPa K^{-1} (Helffrich, 2000). Thus, if the 410 and 660 km discontinuities are entirely due to these phase transformations, regions of abnormally low temperature such as subduction zones should correspond to elevation of the 410 to lower depths and depression of the 660 to greater depths (Figure 2). In general, the 660 is depressed under cold regions (slabs) as expected, but the 410 appears to be far more complicated (Gu et al., 1998; Flanagan and Shearer, 1998a, b).

Converting the pressure change to the depth, the vertical displacement of this phase change is:

$$\lambda = \frac{dP}{dT} \quad , P = \rho g Z \Rightarrow \frac{dZ}{dT} = \frac{\lambda}{\rho g} \qquad (2)$$

Z is the vertical displacement (equation 2).

Teleseismic receiver function analysis is a powerful tool to study the upper mantle discontinuities beneath seismic station (Vinnik 1977; Li et al., 2000a, b). A teleseismic P wave impinging on a discontinuity beneath a seismic station, will produce a converted shear wave which follow the P wave with some delay. The time difference between the conversions of the two discontinuities is independent of the shallow mantle structure and therefore indicates the thickness of the transition zone. By comparing this differential time with the global average value (24.0s for the IASP91 model at a reference distance of 67˚), it is possible to estimate the variation in thickness of the mantle transition zone (MTZ) and the temperature variation in the ambient mantle. Therefore, the variation in the transition zone thickness (TZT) can be used to infer the temperature variation there (Li et al., 2003). For an excess temperature of about 200˚ C, the TZT can be reduced by about 20-30 km (Helffrich, 2000).

There are some independent estimates of the crustal thickness beneath the NW Iran (e.g. Asudeh, 1982a; Dehghani & Makris, 1984; Seber et al., 1997; Gheitanchi, 1996; Mooney et al., 1998, Bassin et al., 2000; Bayramnejad, 2008; Taghizadeh-Farahmand et al., 2008).Thickness of the lithosphere has been mostly studied by low resolution surface waves (e.g. Priestley and McKenzie, 2006; McKenzie and Priestley, 2007). A recent study by Taghizadeh-farahmand et al. (2010), based on S receiver function, indicates a lithosphere thickness of ~85 km beneath the NW Iran. But there is any study on transition zone's discontinuities in NW Iran.

The main goal of this paper is to investigate of the transition zone's discontinuities of upper mantle in the NW Iran using P receiver function.

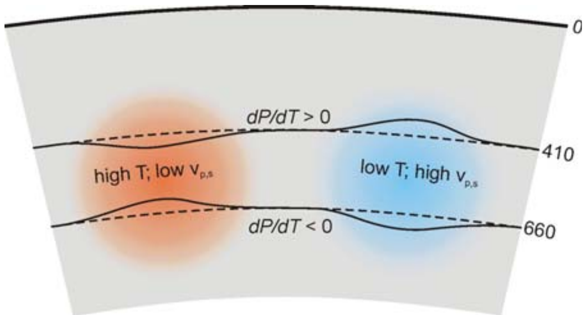

Figure2. Schematic depiction of the mantle transition zone in an olivine-dominant mantle after Lebedev et al. (2002). The transition from olivine to wadsleyite and from spinel to perovskite and magnesiowüstite give rise to the 410- and 660-km discontinuities, respectively. The effective Clapeyron slopes dP/dT have opposite signs. Absent lateral variations in composition, relatively low temperatures (T) cause thickening of the transition zone and increase in seismic velocities (vp, vs), while high temperatures cause thinning of the transition zone and decrease in vp and vs.

2 Data and Methodology

The Tabriz Telemetry Seismic Network consists of 8 three-component short period stations (AZR, BST, HRS, HSH, MRD, SHB, SRB and TBZ). Figure 1 shows the setup of the Tabriz Telemetry Seismic Network and Table 1 lists station names and coordinates. These stations are equipped with SS-1 seismometers with natural frequency of 1HZ made by Nanometrics of Canada. The data is recorded on a 50-samples-per-second. We selected teleseismic events (about 350 events) with Mb ≥ 5.5, epicentral distance between 30°- 95° recorded from 1995 to 2008 for P receiver function analysis (Figure 3). Methodology (P receiver function analysis) used in this paper is the same as described by Sodoudi et al. (2006b).

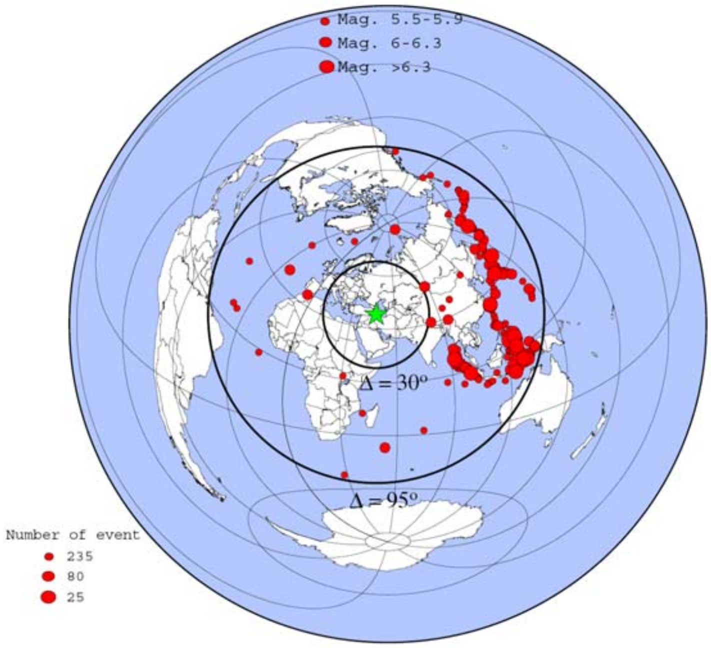

Figure3. The epicenter distribution of events used to this study which recorded by Tabriz Telemetry Seismic Network from 1995 to 2008. The green star shows center of Tabriz Telemetry Network. The black solid circles mark the 30° and 90° epicentral distances, respectively.

Table1. Specification of the seismic stations is shown in Figure1.

Station name	Station code	Latitude Deg.	Longitude Deg.	Elevation (m)	Number of PRF
Azarshahr	AZR	37.6783	45.9800	2300	54
Bostanabadb	BST	37.7000	46.8917	2100	38
Hashtroud	HSH	37.3067	47.2633	2850	15
Heris	HRS	38.3183	47.0417	2100	23
Marand	MRD	38.7133	45.7033	1684	70
Sarab	SRB	37.8250	47.6667	1950	28
Shabestar	SHB	38.2833	45.6166	2150	35
Tabriz	TBZ	38.2333	46.1466	1650	41

3 P RECEIVER FUNCTION ANALYSES

P waveform data with relatively high signal-to-noise ratio have been carefully selected at each station from teleseismic earthquake. We considered a time window of 110s, starting 10 s before the P-onset arrival time. Firstly, to broaden the response of short-period instruments into a more useful teleseismic frequency band, the instrument response is denconvolved from the original records. ZNE components are then rotated into the local LQT ray-based coordinate system. A band-pass filter of 2-10s is applied to the P receiver functions (PRFs). They are stacked after move out correction for a reference slowness of 6.4 s/°.

4 DISCUSSION AND CONCOLUSION

We calculated PRFs for all stations. Individual and summed PRFs for all stations are presented in Figure 4. The traces for all station are arranged with increasing longitude of piercing points.

The obtained 2D migrated section along 38˚ longitude (Figure 6) is represented in Figure 5. In the migration process, each signal receiver function is back-projected along its path. The paths are calculated using the IASP91 reference model (Kennet and Engdahl, 1991). The positive amplitudes of receiver functions are plotted in red, while blue color shows negative amplitudes. As Figure 5 shows, the transition zone's discontinuities of upper mantle are visible. Those discontinuities (410 and 660 km) are not flat and have anomaly near and under volcanoes and have derived from the standard IASP91 global earth model. Both discontinuities appear to be depressed in the central portion of the profile.

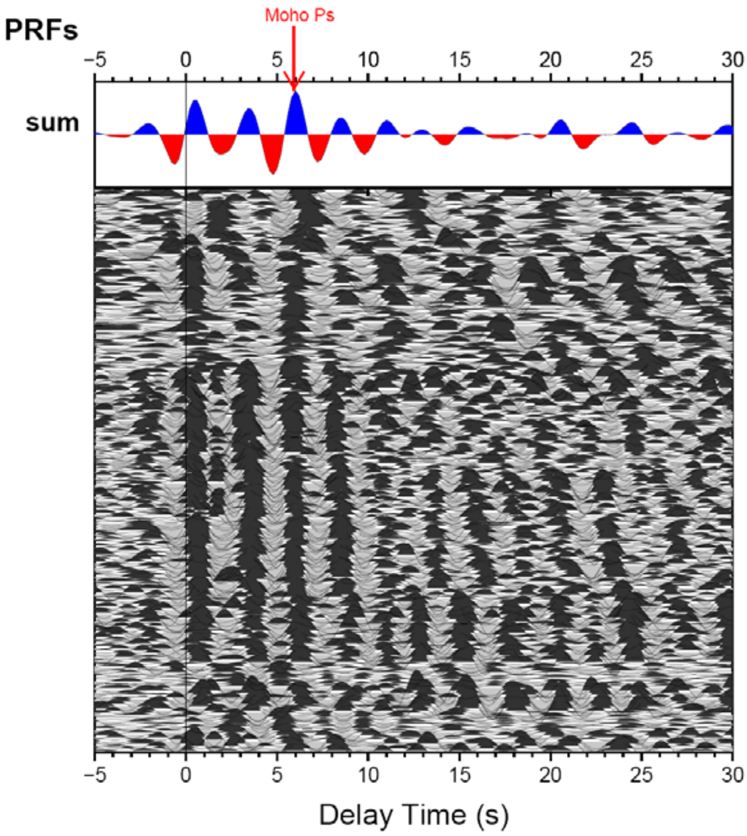

Figure4. Individual PRFs with summation traces for all stations. The PRFs are plotted equally spaced and sorted by increasing piercing points of Ps. The P onset is fixed at zero time. Red arrow shows the P-to-S converted phase from the Moho (labeled Moho Ps on the summation traces).

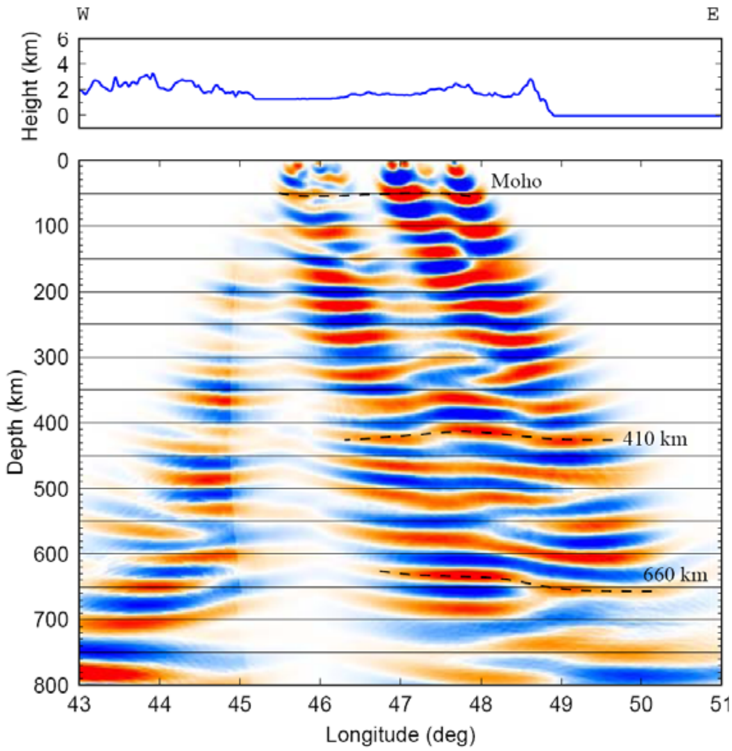

Figure5. 2D migrated image of the PRFs along a WE profile, The topography along the profile is also indicated at the top. The positive amplitudes of receiver function are plotted in red, while blue color shows negative amplitudes.

In order to investigate the 410 and 660 with the receiver function data, it is necessary to take into account that due to the ray geometry. Figure 6 shows the distribution of the P-to-S piercing points at 410 and 660 km depth. The P-to-S conversion points are located close to the stations (black inverse triangles).

The amplitudes of Ps conversions from the upper mantle discontinuities are about four times weaker than the Moho Ps conversion signal (Heuer, 2006) ,due to the attenuation and scattering of weak converted phases that originate from the mantle discontinuities and travel through the heterogeneous upper mantle and crust, it is necessary to stack receiver functions. Before stacking, a distance moveout correction is applied using the IASP91 global reference model and a reference slowness of 6.4s/° permitting summation of records from different distances. In order to enhance the conversions and reduce the error of the depth determination, we stacked the PRF in bins of 0.09° (overlapping factor of 0.07°) and sorted them by latitiude of piercing points at 410 km depth (Figure 6). The stacking method gained the P-to-S conversions by averaging the information of several single PRF within each bin. Negative (positive) amplitudes, plotted in gray (black) indicate a velocity decrease (increase) with depth. Different filters were tested beforehand in order to enhance the signals of the 410 and 660. This led to the choice of a bandpass filter between 5-20 s. Theoretical times of theses two phases for the IASP91 model are 44.1 and 68.1 s (differential time is 24.0 s) at 67˚ (or 6.4 ˚/s slowness). There are showed black lines in Fig.7. The sum trace of all individual traces shows the Ps conversion signal from the 410 at 46 s and 660 at 69 s, which is 1.92s and 0.92s later than predicted by the IASP91 reference model, respectively. Furthermore, a signal at 52 s delay time, which may be attributed to the discontinuity at 520 km depth, is visible in the sum trace of Figure 7.

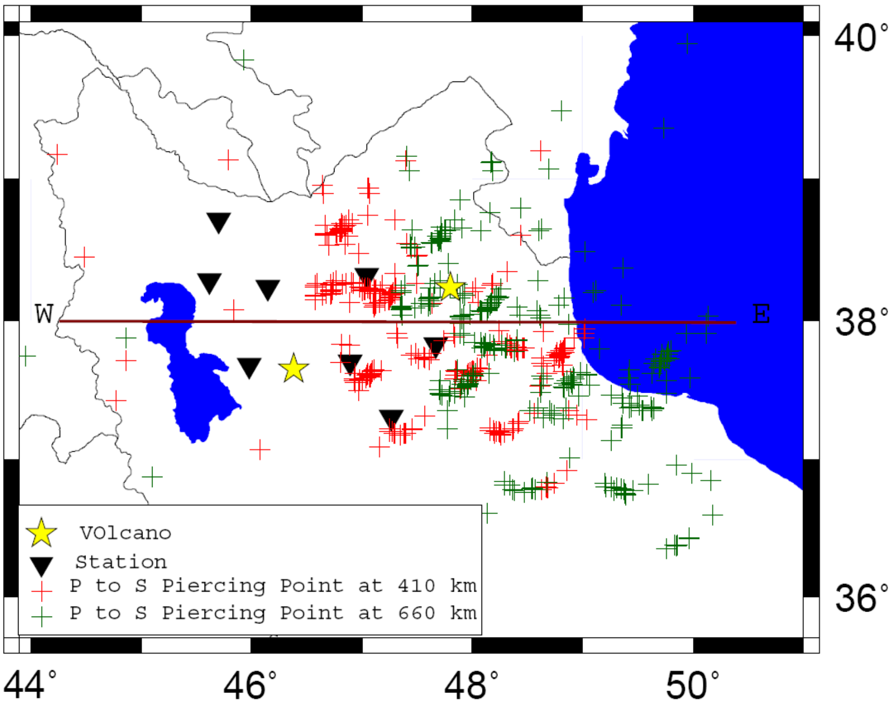

Figure6. Piercing points of the P-to-S converted phases at interfaces at 410 km (red pluses) and 660 km (green pluses). Black inverse triangles denote stations and yellow stars are volcano.

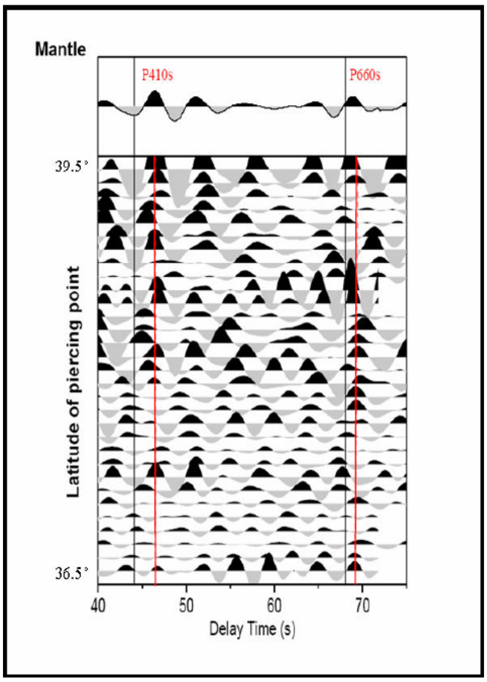

Figure7. Stacked receiver functions of boxes with piercing points at 410 km depth. The single traces were moveout corrected and filtered between 5-20 s before stacking. Gray Lines at 44.08 s and 68.08 s mark the delay times of the 410 and 660 km discontinuities according to the IASP91 reference model. Coherent positive arrivals near the delay times predicted by IASP91 are clearly visible for both the 410 and 660 (marked as P410s and P660s).

The signal can be followed through most of the individual boxes and appears to be rather coherent. The differential time between both discontinuities is 23 s and less than IASP91 model. Because the 410 and 660 km discontinuities do not show the same delay, the transition zone is still thinner, which is probably resulted temperature anomaly and caused decrease in seismic velocities (Vp, Vs). Over the last decade, a number of seismic studies have examined the crust and upper mantle structure beneath the Middle East. Large-scale surface wave tomography studies have shown variable crustal thickness and upper mantle velocities (Ritzwoller and Levshin, 1998; Pasyanos et al., 2001; Villasenor et al., 2001; Pasyanos and Walter, 2002; Shapiro and Ritzwoller, 2002; Alinaghi et al., 2007; Reiter and Rodi, 2006). Also Tomographic studies (Bayramnejad, 2008) indicated a significant LVZ beneath the volcanoes in NW Iran. They showed a depth of about 12 and 15 km for the LVZ beneath the Sabalan and Sahand volcanoes, respectively. It could mean, plume lift and there is temperature anomaly in transition zone beneath NW Iran, as result transition zone is become thin (according Fig. 2). Therefore, our result derived from P receiver function is in good agreement with results from Bayramnejad (2008). Regarding previous studies in this region (Hearn and Ni 1994; Ritzwoller et. al., 1998; Al-Lazki et. al., 2003, 2004; Phillips et. al., 2007; Ozacar et. al., 2008) slow Pn velocities (≤ 8 km/s) is acceptable. Nafi Toksöz et. al., 2010 and Shunping Pei et. al., 2010 showed that Low P and S velocities beneath NW Iran in the Crust and upper mantle (e. g. depths of 200, 400 and 660 km) which is the adjusted our result.

With the deployment of temporary three-component seismic stations in NW Iran, teleseismic P-to-S converted waves have been studied to map the upper mantle 410 km and 660 km discontinuities. The two global discontinuities at 410 and 660 km are observed but the timings are delayed by about 2 and 1 s relative to the IASP91 global reference model. The conversion times of the 410 km discontinuity are late for a typical continental upper mantle (Li et al., 2003), indicating that the upper mantle NW Iran is warm and 3-4 % slower than the standard model. This would indicate that the upper mantle across the NW Iran is still strongly influenced by several geodynamical processes involving rifting, uplift and magmatism above the transition zone and below the Moho.

Acknowledgments

Authors are grateful to the Institute of Geophysics, Tehran University for providing the teleseismic waveforms. We used the software packages SeismicHandler (Stammler, 1993) for data processing and GMT (Wessels and Smith, 1998) for plotting, respectively.

REFERENCE:

Alinaghi, A., Koulakov, I., and Thybo, H., 2007, Seismic tomographic imaging of P- and Swaves velocity perturbations in the upper mantle beneath Iran, Geophysical Journal International, **169**(3), 1089-1102.

Al-Lazki, A., Sandvol., E., Seber, D., Barazangi, M., and Turkelli, N., 2003, Pn tomographic imaging of mantle lid velocity and anisotropy at the junction of the Arabian, Eurasian, and African plates, Geophys. Res. Lett., **30**, doi: 10.1029/2003GL017391.

Al-Lazki, A. I., Sandvol, E., Seber, D., Barazangi, M., Turkelli, N., and Mohamad, R., 2004, Pn tomographic imaging of mantle lid velocity and anisotropy at the junction of the Arabian, Eurasian and African plates, Geophys. J. Int., **158**, 1024-1040.

Asudeh, I., 1982a, Seismic structure of Iran from surface and body wave data, Geophys. J. R. Astr., **71**, 715-730.

Bassin, C., Laske, G., and Masters, G., 2000, The current Llimits of resolution for surface wave tomography in North America, EOS Trans AGU., **81,** F897.

Bayramnejad, E., 2008, Determination of crustal velocity structure in NW Iran using 3-D inverse modeling of local earthquake data, Tehran University, Ph.D thesis.

Bercovici, D., and Karato, S. I., 2003, Whole-mantle convection and the transition-zone water filter, Nature, **425**, 39-44.

Bina, C. R., and Helffrich, G. R., 1994, Phase transition Clapeyron slopes and transition zone seismic discontinuity topography, J. Geophys. Res., **99**, 15 853-15 860.

Dehgani, G. A., and Makris, J., 1984, The gravity field and crustal structure of Iran, N. Jb. GeoL. Palaont Abh., **168**, 215-229.

Deuss, A., and Woodhouse, J. H., 2001, Seismic observation of splitting of the mid-transition zone discontinuity in Earth_s Mantle, Science, **294**, 354-357.

Flanagan, M. P., and Shearer, P. M., 1998a, Global mapping of topography on transition zone velocity discontinuities by stacking SS precursors, J. Geophys. Res., **103**, 2673- 2692.

Flanagan, M. P., and Shearer, P. M., 1998b, Topography on the 410 km seismic velocity discontinuity near subduction zones from stacking of sS, sP and pP precursors, J. Geophys. Res., **103**(21) 165-182.

Gaherty, J. B., Kato, M., and Jordan, T. H., 1999, Seismological structure of the upper mantle: a regional comparison of seismic layering, Phys. Earth Planet. Inter., **110**, 21-41.

Gheitanchi, M. R., 1996, Crustal structure in NW in Iran, revealed from the 1990 Rudbar aftershock sequence, J. Earth & Space Phys., **23**, 7-14.

Gheitanchi, M. R., Mirzaei, N., and Bayramnejad, E., 2004, Pattern of seismicity in Northwest Iran, revealed from local seismic network, Geoscience, **11**, 104-111.

Gossler, J., and Kind, R., 1996, Seismic evidence for very deep roots of continents, Earth Planet. Sci. Lett., **138**, 1-13.

Gu, Y., Dziewonski, A. M., and Agee, C. B., 1998, Global de-correlation of the topography of transition zone discontinuities, Earth Planet. Sci. Lett., **157**, 57-67.

Hearn, T. M., and Ni, J., 1994, Pn velocities beneath continental collision zones: The Turkish- Iranian plateau, Geophys. J. Int. **117**,273-283.

Helffrich, G. R., 2000, The Earth_s mantle, Rev. Geophys., **38**, 141-158.

Hessami, K., Pantosti, D., Tabasi, H., Shabanian, E., Abbasi, M. R., Feghhi, K., and Soleymani, S., 2003, Paleoearthquakes and slip rates of the North Tabriz Fault, NW Iran: preliminary results, Annals of Geophysics, **46**, 903-915.

Heuer, B., 2006, Lithospheric and mantle structure beneath the western Bohemian Massif obtained from teleseismic P and S receiver functions, FU Berlin, PhD thesis, **146**p.

Kennett, B. L. N., and Engdahl, E. R., 1991, Travel times for global earthquake location and phase identification, Geophys. J. Int., **105**, 429-465.

Lebedev, S., Chevrot, S., and van der Hilst, R. D., 2002, Seismic evidence for olivine phase changes at the 410- and 660-kilometer discontinuities, Science, **296**, 1300-1302.

Li, X., Kind, R., Priestley, K., Sobolev, S. V., Tilmann, F., Yuan, X., and Weber, M., 2000a, Mapping the Hawaiian plume with converted seismic waves, Nature, **405**, 938-941.

Li, X., Sobolev, S. V., Kind, R., Yuan, X., and Estabrook, C., 2000b, A detailed receiver function image of the upper mantle discontinuities in the Japan subduction zone, Earth Planet. Sci. Lett., **186**, 527-541.

Li, X., Bock, G., Vafidis, A., Kind, R., Harjes, H. P., Hanka, W., Wylegalla, K., Meijde, M., and Yuan, X., 2003, Receiver function study of Hellenic subduction zone: Imaging crustal thickness variations and the oceanic Moho of the descending African lithosphere, Geophys. J. Int., **155**, 733-748.

McKenzie, D., and Priestley, K., 2007, The influence of lithospheric thickness variations on continental evolution, Lithos., **01584**, 11p.

Mooney, W. D., Laske, G., and Masters, G., 1998, A global crustal model at 5 × 5 degree, J. Geophys. Res., **103**, 727-747.

Ozacar, A. A., Gilbert, H., and Zandt, G., 2008, Upper mantle discontinuity structure beneath East Anatolian Plateau (Turkey) from receiver functions, Earth and Planetary Science Letters, **269**, 426-434.

Pasyanos, M. E., Walter, W. R., and Hazler, S. E., 2001, A surface wave dispersion study of the Middle East and North Africa for monitoring the comprehensive Nuclear-Test-Ban Treaty, Pure Appl. Geophys, **158**, 1445-1474.

Pasyanos, M. E., and Walter, W. R., 2002, Crust and upper mantle structure of North Africa, Europe, and the Middle East from inversion of surface waves, J. Geophys. Int. **149**, 463-481.

Phillips, W. S., Begnaud, M. L., Rowe, C. A., Steck, L. K., Myers, S. C., Pasyanos, M. E., and Ballard, S., 2007, Accounting for lateral variations of the upper mantle gradient in Pn tomography studies, Geophys. Res. Lett., **34**, L14312, doi: 10.1029/2007GL029338.

Priestley, K., and McKenzie, D., 2006, The thermal structure of lithosphere from shear wave velocities, Earth and Planetary Sci. Lett. **244**, 285-301.

Reiter, D., and Rodi, W., 2006, Crustal and upper-mantle P- and S-velocity structure in central and southern Asia from joint body-and surface-wave inversion, in Proceedings of the 28th Seismic Research Review: Ground-Based Nuclear Explosion Monitoring Technologies, LA-UR-06-5471, **1**, 209-218.

Ringwood, A. E., and Major, A., 1966, High-pressure transformations in pyroxenes, Earth Planet. Sci. Lett., **1**, 241-245.

Ritzwoller, M., and Levshin, A., 1998, Eurasian surface wave tomography: group velocities, J. Geophys. Res., 103, 4839-4878.

Ritzwoller, M., Levshin, A., Ratnikova, L., and Egorkin, A., 1998, Intermediate-period groupvelocity maps across Central Asia, western China, and parts of the Middle East, Geophys. J. Int., 134, 315-328.

Rost, S., and Weber, M., 2002, The upper mantle transition zone discontinuities in the Pacific as determined by short-period array data, Earth Planet. Sci. Lett., **204**, 347-361.

Seber, D., Vallve, M., Sandvol, E., and Steer, D., 1997, Middle East Tectonics: Applications of Geographic Information Systems (GIS), GSA Today.

Shapiro, N. M., and Ritzwoller, M. H., 2002, Monte-Carlo inversion for a global shear velocity model of the crust and upper mantle, Geophys. J. Int., 152, 88-105.

Shearer, P. M., 1990, Seismic imaging of upper-mantle structure with new evidence for a 520-km discontinuity, Nature, **344**, 121-126.

Shearer, P. M., and Masters, T. G., 1992, Global mapping of topography on the 660-km discontinuity, Nature, **355**, 791-796.

Shearer, P. M., 1996, Transition zone velocity gradients and the 520-km discontinuity, J. Geophys. Res., **101**(B2), 3053-3066.

Pei, S., Sun, Y., and Toksöz, M. N., 2010, Tomographic Pn and Sn Velocity beneath continental collision zone in Middle East and Middle Asia, submitted to the Journal of Geophysical Research.

Sodoudi, F., Kind, R., Priestly, W., Hanka, W., Wylegalla, K., Stavrakakis, G., Vafidis, A., Harjes, H. P., and Bohnhoff, M., 2006, Lithospheric structure of the Aegean obtained from P and S receiver functions, J. Geophys. Res., **111**, 12307-12330.

Stammler, K., 1993, Seismichandler-Programmable multichannel data handler for interactive and automatic processing of seismological analyses. Computer & Geosciences, **19**, 135-140.

Taghizadeh-Farahmand, F., Sodoudi, F., Ghietanchi, M. R., and Kaviani, A., 2008, Crustal structure beneath Northwest Iran using teleseismic converted waves, J. Earth Science (GSI), **68**, 131-136.

Taghizadeh-Farahmand, F., Sodoudi, F., Ghietanchi, M. R., and Afsari, N., 2010, The lithosphere- asthenosphere boundary in the North-West of Iran from S receiver function, J. Earth & Space Phys., **35**, 1-13.

Toksöz, M. N., Van der Hilst, R. D., Sun, Y., and Zhang, H., 2010, Seismic tomography of the Arabian-Eurasian collision zone and surrounding areas, AIR FORCE RESEARCH LABORATORY, Space Vehicles Directorate 29 Randolph Rd, AIR FORCE MATERIEL COMMAND HANSCOM AFB, MA 01731-3010.

Wessel P, and Smith, W. H. F., 1998, New improved version of the Generic Mapping Tools Released. EOS Trans. AGU, **79**, 579.

Villasenor, A., Ritzwoller, M. H., Levshin, A. L., Barmin, M. P., Engdahl, E. R., Spakman, W., and Trampert J., 2001, Shear velocity structure of central Eurasia from inversion of surface wave velocities, Physics of the Earth and Planetary Interiors 123, 169-184.

Vinnik, L. P., 1977, Detection of waves converted from P to Sv in the mantle, Phys. Earth planet. Intre., **15**, 39-45.